



ORIGINAL ARTICLE

Cyclodextrin modified with different groups to enhance the drug delivery efficiency of gold nanoparticles to treat cancer



Cao-Hien Nguyen^{a,b,1}, Kien-Sam Banh^{c,1}, Tran Nguyen Minh An^d,
Nguyen Thi Hong Anh^a, Chi-Hien Dang^{b,c,*}, Van-Dat Doan^d, Tran Thi Kim Chi^e,
Hieu Vu-Quang^f, Thanh-Danh Nguyen^{b,c,*}

^a Department of Chemical Technology, Ho Chi Minh City University of Food Industry, 140 Le Trong Tan, Tan Phu District, Ho Chi Minh 72000, Vietnam

^b Graduate University of Science and Technology, Vietnam Academy of Science and Technology, 18 Hoang Quoc Viet, Cau Giay, Hanoi 11000, Vietnam

^c Institute of Chemical Technology, Vietnam Academy of Science and Technology, 1A, TL 29, Thanh Loc Ward, District 12, Ho Chi Minh City 700000, Vietnam

^d Faculty of Chemical Engineering, Industrial University of Ho Chi Minh City, Ho Chi Minh City 71420, Vietnam

^e Institute of Materials Science, Vietnam Academy of Science and Technology, 18 Hoang Quoc Viet, Cau Giay District, Hanoi 11000, Vietnam

^f NTT Hi-Tech Institute, Nguyen Tat Thanh University, Ho Chi Minh City 700000, Vietnam

Received 14 February 2023; accepted 10 June 2023

Available online 17 June 2023

KEYWORDS

Breast anticancer;
Modified β -cyclodextrin;
Gold nanoparticles;
5-fluorouracil;
Drug delivery;
Molecular docking model

Abstract The aim of this research is to investigate the influence of different functional groups of β -cyclodextrin (CD) in functionalizing gold nanoparticles. The functionalized nanoparticles are then utilized for loading the 5-fluorouracil (5-FU) drug and evaluating their *in vitro* anticancer activity. A two-step method was employed to synthesize Mono-6-(1,3-trimethylenediamine)-6-deoxy- β -cyclodextrin (TMACD), which was further utilized for fabricating gold nanoparticles (AuNPs) using ultrasound-assisted synthesis. To investigate effect of different functional groups of β -cyclodextrin (CD) on drug delivery efficiency, three cyclodextrin derivatives, namely β -cyclodextrin (5-FU@AuNPs/CD), 2-hydroxypropyl- β -cyclodextrin (5-FU@AuNPs/HPCD), and TMACD (5-FU@AuNPs/TMACD) were utilized to load 5-FU. Among them, the

* Corresponding authors.

E-mail addresses: dangchihien@gmail.com (C.-H. Dang), ntdanh@ict.vast.vn (T.-D. Nguyen).

¹ These authors contributed equally to this study.

Peer review under responsibility of King Saud University.



nanocomposite AuNPs/TMACD exhibited the highest associate efficiency and loading efficiency which were confirmed by analytic techniques such as FTIR, PXRD, TEM. Moreover, the release behavior of 5-FU from the nanocomposites was investigated at pH 7.4, revealing that all AuNPs/CDs nanocomposites effectively protected the drug with a low release percentage ranging from 23.13% to 29.45%. Docking model analysis indicated that the 5-FU ligand formed six hydrogen bonds and interacted favorably with the HPCD molecule. In the *in vitro* cell viability assay, both nanocomposites, 5-FU@AuNPs/CD and 5-FU@AuNPs/TMACD, not only demonstrated effective anticancer activity against breast cancer cells (MCF-7) but also exhibited minimal toxicity towards normal cell lines. Remarkably, the results revealed that 5-FU@AuNPs/TMACD displayed the highest efficacy in suppressing the growth of the breast cancer cells. These findings highlight the considerable potential of amine-derivative cyclodextrin-capped AuNPs as exceptionally efficient carriers for anticancer drugs, offering promising applications in both diagnosis and therapy.

© 2023 The Author(s). Published by Elsevier B.V. on behalf of King Saud University. This is an open access article under the CC BY-NC-ND license (<http://creativecommons.org/licenses/by-nc-nd/4.0/>).

1. Introduction

Gold nanoparticles (AuNPs) find extensive applications in various multidisciplinary fields such as optoelectronics, nanomedicine, and sensing (Elahi et al., 2018, Ali et al., 2021). AuNPs possess many promising physicochemical characteristics including electronic, optical, and biological properties (Gu et al., 2021, Ielo et al., 2021). Recent studies have demonstrated that inorganic AuNPs functionalized with drug molecules have shown increased therapeutic performance of drugs. In such case, the drugs could be released from the surface of AuNPs *via* desorption or protonation in low pH (Kim et al., 2009, Ajnai et al., 2014). However, this approach often necessitates chemical modification of the drugs to anchor them to the surface of inorganic nanoparticles which imposes limitations on the therapeutic vehicles of the drug (Kumar et al., 2013, Jeong et al., 2014). Consequently, the utilization of AuNPs with organic stabilizing agents offers several advantages, including incorporating drugs into their structure and increasing the drug loading efficiency (Nejati et al., 2021, Sathiyaseelan et al., 2021).

The synthesis of functionalized AuNPs involves the reduction of metallic salts using reducing agents in the presence of stabilizers. Numerous stabilizers, such as chitosan, alginate, cellulose, and cyclodextrin (CD), are routinely used in the synthesis of AuNPs due to their biocompatible properties (Chen et al., 2020, Bulut and Yilmaz 2021, Ho et al., 2021). These compounds play a crucial role in preventing nanoparticle agglomeration and controlling the size of metallic nanoparticles (Nguyen et al., 2019). Functionalized AuNPs, owing to their excellent biocompatibility and ease of functionalization for target site recognition, have found applications in drug delivery systems for disease diagnosis and therapy (Daraee et al., 2016, Chen and Feng 2022). Our research group recently reported a straightforward method for the fabrication of CD-capped AuNPs under the assistance of ultrasound in an alkaline condition (Nguyen et al., 2022). In this study, CD was utilized both as the reducing agent and stabilizer without the use of other chemicals.

Cyclodextrins, are cyclic polysaccharides composed of repeating *D*-glucopyranose units. They are non-toxic, biocompatible, and environmentally friendly, making them widely used in pharmaceutical and food fields (Mohandoss et al., 2020, Tarannum and Kumar 2020). CD-mediated delivery systems utilize host–guest interactions to effectively deliver drugs to target sites, due to the reversible release of hydrophobic drugs in the system (Hu et al., 2014). α -, β -, and γ -CDs, consisting of six, seven, and eight glucopyranose units, respectively, have been shown to interact well with anticancer drugs. For examples, Lu et al. (Lu et al., 2016) demonstrated that among cyclic molecules, β -CD loaded with phthalocyanines had the highest anticancer activity compared to other complexes. Donato et al. (Di Donato et al., 2016) showed that both α - and β -CDs could effectively

load 5-FU in their inner cavities, as confirmed by docking analysis. The complex with β -CD showed the highest cytotoxic activity on the mouse breast cancer cell line (MCF-7), while the complex with α -CD had the highest cytotoxicity effect against the leukemia cell line (A-549). β -CD derivatives such as HPCD (Chowdhury et al., 2019) or methyl- β -cyclodextrin (Yang et al., 2018) have been used for the complexation of anticancer drugs, but the interaction of these derivatives with drugs has not been systematically investigated. As a result, CD-based nanoparticles have been extensively investigated for loading the 5-FU drug in cancer cell treatment. Various approaches have been employed, including the preparation of 5-FU@CD nanoplexes through crosslinking methods using epichlorohydrin, which exhibited good bioactivity against CT26 mouse colon carcinoma cells (Akkin et al., 2022). Additionally, the 5-FU@ β -CD/alginate nanocomposite demonstrated efficacy against breast cancer cells (MCF-7) (Nguyen et al., 2022).

On the other hand, CDs can be modified and used as stabilizing agents for the fabrication of AuNPs in drug delivery applications (Liu et al., 2003, Male et al., 2008, Heo et al., 2012, Shi et al., 2013, Arockia Jency et al., 2015). Park et al. (Park et al., 2009) have functionalized AuNPs using thiol-CD and α -methoxy- ω -mercapto-poly(ethylene glycol) for encapsulation of β -lapachone. This drug can be controllably released in glutathione medium. However, thiol group (SH) can increase the toxic risk which impede usage of the drugs in disease therapy. CD derivatives bearing functional groups with low toxicity such as amine and hydroxyl groups, are a feasible solution for this issue. Recently, Lakkakula et al. (Lakkakula et al., 2021) showed that 5-FU@HPCD complex stabilized AuNPs exhibited good bioactivity against breast cancer cells. However, to the best of our knowledge, influence of CD functional groups on AuNPs and their applications in drug delivery systems have not been explored so far.

In this work, we aimed to investigate the impact of hydroxyl and amine groups in β -CD on the nanocomposite AuNPs/CDs for loading. Furthermore, we assayed the toxicity of the nanocomposite to cell lines and explored the chemical interaction between 5-FU and CD molecules using an *in silico* docking model.

2. Materials and methods

2.1. Materials

β -cyclodextrin (CD), (2-hydroxypropyl)- β -cyclodextrin (HPCD) and chloroauric acid hydrate (HAuCl₄·xH₂O) were purchased from Acros Co. (Belgium). Solvents was purchased from Chemsol (Vietnam). Other reagents were provided by Sigma Co. (USA). CH₂Cl₂ using for the synthesis was distilled

in anhydrous CaCl₂. β -CD was dried at 60 °C in oven under vacuum for 2 h before the synthesis. Deionized water was used thoroughly in all experiments.

2.2. Synthesis of mono-6-(1,3-trimethylenediamine)-6-deoxy- β -cyclodextrin (TMACD)

2.2.1. Mono-6-(*p*-toluensulfonyl)-6-deoxy- β -cyclodextrin (TsCD)

1-tosyl-1H-imidazole (TsIm). In a 1L-round bottom flask, 10 g tosyl chloride (52.5 mmol) and 8 g imidazole (118 mmol) were added to 500 mL of CH₂Cl₂ under nitrogen atmosphere at 0 °C. After 4 h, the mixture was filtered flash through a silica gel column with solvent mixture of ethyl acetate/hexane (1:1). The solvent was evaporated under vacuum. The residue was recrystallized in ethyl acetate/hexane (1:10) to afford pure 1-tosyl-1H-imidazole (TsIm) (10.6 g, 91%). White powder. ESI-MS (*m/z*): 223.55 [M + H]⁺ calcd for C₁₀H₁₁N₂O₂S ([M] = 222.26). ¹H NMR (500 MHz, DMSO, *ppm*): δ 8.01 (*s*, 1H), 7.83 (*d*, *J* 8.5 Hz, 2H), 7.36 (*d*, *J* 8.0 Hz, 2H); 7.29 (*s*, 1H); 7.08 (*s*, 1H); 2.43 (*s*, 3H). ¹³C NMR (125 MHz, CDCl₃, *ppm*): δ 146.3, 136.7, 135.0, 131.4, 130.4, 127.3, 117.5, 21.7.

Mono-6-(p-toluensulfonyl)-6-deoxy- β -cyclodextrin (TsCD). 8.9 g TsIm (40 mmol), 35 g β -cyclodextrin (30.84 mmol) and 350 mL H₂O were added into 3-necks round bottom flask (1L) and stirred for 4 h at room temperature (RT). Then, NaOH solution (50 mL, 20%) was added to the mixture and stirred additionally 10 min. The mixture was filtered to remove solid. The filtrate was neutralized to pH 7 by NH₄Cl solution (1 M). The precipitated solid was filtered and washed with water. The product was dried in vacuum at RT (21 g, 52%). White powder, purity (99%, HPLC). m.p. 177 °C-178 °C. R_f (*n*-butanol:ethanol:H₂O = 5:4:3) = 0.49. QTOF-MS (*m/z*): 1311.3664 [M + Na]⁺ calcd for C₄₉H₇₆O₃₇SNa ([M + Na]⁺ = 1311.3684). FTIR (*v*_{max}, *cm*⁻¹, *KBr*): 3386 (O-H), 2927 (C-H), 1645 and 1365 (C = C), 1157 (SO₂) and 1029 (C-O). ¹H NMR (500 MHz, DMSO *d*₆, *ppm*): δ 7.75 (*d*, *J* 8.0 Hz, 2H), 7.43 (*d*, *J* 8.0 Hz, 2H), 5.80–5.62 (*m*, 14H), 4.84–4.76 (*m*, 7H), 4.48–4.18 (*m*, 8H), 3.65–3.21 (*m*, 34H), 2.43 (*s*, 3H). ¹³C NMR (125 MHz, DMSO *d*₆, *ppm*): δ 144.8, 132.7, 129.9, 127.6, 102.3, 102.0, 101.9, 101.3, 81.7, 81.6, 81.5, 81.2, 80.8, 73.1, 72.2, 72.1, 71.9, 69.7, 68.9, 59.9, 59.8, 59.6, 59.3, 21.2.

2.2.2. Mono-6-(1,3-trimethylenediamine)-6-deoxy- β -cyclodextrin (TMACD)

TsCD (1.5 g, 1.16 mmol) and 1,3-diaminopropane (9.76 mL, 116 mmol) were added to a 100 mL round bottom flask. The mixture was irradiated microwave (SANYO EM-G205AW) at 300 W for 12 min. Ethanol (600 mL) was added to obtain a white precipitate. The solid was collected by filtration and washed with ethanol to afford the product TMACD (0.65 g, 47%). White powder, purity (99.9%, HPLC). M.p. 259–260 °C. R_f (*n*-butanol:ethanol:H₂O = 5:4:3) = 0.49. QTOF-MS (*m/z*): 1191.4457 [M + H]⁺ calcd for C₄₅H₇₉O₃₄N₂ ([M + H]⁺ = 1191.4514). IR (*v*_{max}, *cm*⁻¹, *KBr*): 3417 (O-H), 2927(C-H), 1642 và 1525 (N-H), 1031 (C-O). ¹H NMR (500 MHz, D₂O, *ppm*): δ 5.05 (*s*, 7H), 3.94–3.82 (*m*, 32H), 3.64–3.53 (*m*, 14H), 3.42–3.39 (*m*, 1H), 3.09–3.03 (*m*, 1H), 2.79 – 2.75 (*m*, 4H), 2.63–2.61 (*m*, 2H), 1.71–1.68 (*m*, 2H), 1.17 (*t*, *J* 7.0 Hz, 2H, NH₂). ¹³C NMR (125 MHz, D₂O, *ppm*): δ 101.9, 81.2, 72.1, 60.4, 54.0, 45.3, 36.6, 30.3.

2.3. Ultrasound-assisted synthesis of gold nanoparticles capped on cyclodextrins

The AuNPs was synthesized from HAuCl₄ in alkaline with CDs as reduced agent and stabilizer under ultrasound assistance (Nguyen et al., 2022). Briefly, HAuCl₄ (11.85 mL, 0.16 mM), 3 mL CDs solution (7 mM) were added into a brown vessel (50 mL) and NaOH solution (1 M) was used to adjust pH 10. The mixtures were irradiated ultrasound irradiation (200 W, 40 kHz, Skymen Ultrasonic Cleaner 6.5L Jp-031, China) at 80 °C for 30 min. The formation of AuNPs was recorded by the UV-Vis measurement (UV-5100, Shanghai Metash Instruments Co.). The solution was added to dialysis bag and washed with water to pH 7.5. Then, the mixture was lyophilized at -80 °C for 24 h. The pink solid products were stored at 4 °C for further study.

2.4. Loading fluorouracil onto the nanocomposites

AuNPs/ β -CD (250 mg) and 5-FU solution (5 mL, 10000 ppm) were stirred in 24 h. The mixture was centrifuged at 4500 rpm for 30 min. The solid was separated and washed with water (10 mL). The nanocomposite product was obtained by lyophilization process (-80 °C, 10 h). The blue solid products were stored at 4 °C for further study.

The association efficiency (AE) is defined as the ratio of drug weight in the nanocomposite to the total drug weight (Eq. (1)).

$$AE(\%) = \frac{W_{total5-FU} - W_{free5-FU}}{W_{total5-FU}} \times 100\% \quad (1)$$

The loading efficiency (LE) of the drug is the ratio of drug weight in the nanocomposite to the dry nanocomposite weight (Eq. (2)).

$$LE(\%) = \frac{W_{total5-FU} - W_{free5-FU}}{W_{nanocomposite}} \times 100\% \quad (2)$$

The 5-FU amount in the supernatant was estimated via a calibration curve of absorbance value at 266 nm in UV-Vis spectroscopy.

2.5. Measurements

NMR and TOF-MS spectra to identify structure of synthesized macromolecules were performed on Bruker Advance 500 NMR spectrometer and SCIEX X500 QTOF, respectively. Zeta potential and dynamic light scattering (DLS) were measured to study the electrochemical equilibrium between the interface and molecular vibration and the particle size distribution in the colloidal solution, respectively. The measurement was performed on a nanoPartica Horiba SZ-100 (Japan) with a solution concentration of 0.5 mg/mL. Zeta potential was determined with an applied voltage of 3.3 V at 25 °C, and DLS was measured at an angle of 173°. Fourier-transform infrared (FTIR) analysis (Tensor 27 FTIR spectrophotometer, Bruker, Germany) was used to analyse functional groups in organic compounds. X-ray diffraction (XRD) patterns of nanocomposite and drug were measured on an X-ray diffractometer, Model-D8 Advance, Bruker (Germany). The morphology and size of the nanocomposites were evaluated using FESEM (S-4800 HI-9057-0006) and TEM (S-4800

JEOL JEM1400). Thermogravimetry analysis (TGA) was performed using a LabSys Evo 1600 (SETARAM, France) in a temperature range from 30 to 800 °C with a heating rate of 10 °C min⁻¹ in air.

2.6. *In silico* molecular docking model

Procedure of docking model was performed by slightly modified method (El-Hachem et al., 2017, Mai et al., 2022) and briefly described in Scheme S1. The active center, spacing, the numbers of elements in X, Y, and Z, axis were (X = 8.485806, Y = -1.655931, and Z = 0.018438), 0.375 Å, (50,50,50), respectively. The grid and dock parameters were set up in grid.gpf and dock.dpf files, respectively. The docking parameters were installed Lamarckian in dock.dpf file and calculation results were in dock.dlg file. The number of models were conducted in 500 times.

2.7. *In vitro* release profile and kinetic analysis of drug

A drug release was studied on a simulated blood fluid with phosphate buffer saline (PBS) at pH 7.4. The drug release efficiency of nanocomposite was explored using a 5 mL dialysis bag as previous report (Nguyen et al., 2022). The nanocomposites (3 mg) and PBS (3 mL) were added to the dialysis bag and immersed in PBS (30 mL) at 37 °C with slow stir. At desired time points, 0.5 mL of dialysis samples from the dialysis cup was collected and the release of drug measured by UV-Vis spectroscopy at 266 nm. The equal amount of PBS was added to the dialysis cup after collecting samples. All experiments were performed in the triplicate. The drug release was calculated via Eq. (3).

$$\text{release}(\%) = \frac{\text{Amount of } 5 - \text{FU at time } t}{\text{Amount of } 5 - \text{FU at time } t = 0} \times 100\% \quad (3)$$

The kinetic models including zero order (Eq. (4)), first order (Eq. (5)), Higuchi (Eq. (6)), Hixson-Crowell (Eq. (7)), and Korsmeyer-Peppas (Eq. (8)) (Rezk et al., 2019, Özkahraman et al., 2023) were applied to investigate the release kinetic profile via an origin software.

$$f_t = k_0 t \quad (4)$$

$$f_t = 1 - e^{-k_1 t} \quad (5)$$

$$f_t = K_H \sqrt{t} \quad (6)$$

$$\sqrt[3]{f_0} - \sqrt[3]{f_t} = K_{HC} t \quad (7)$$

$$f_t = K_{KP} t^n \quad (8)$$

Where f_0 is the initial amount of drug in nanocomposite, f_t is the amount of drug released at a specified time t , n is the diffusion exponent and k_0 , k_1 , K_H , K_{HC} , and K_{KP} are the release constants of the corresponding models.

2.8. Cytotoxicity assay

MCF-7 (HTB-22) and fibroblast cells were provided and cultured by the University of Science, Vietnam National University (Ho Chi Minh City, Vietnam). 5-FU, blank and drug composites were used to test via the SRB assay as previously

reported (Nguyen et al., 2022). Camptothecin and water were used as positive and negative controls, respectively. Cells were seeded into 96-well plates (10,000 cells/well) a day before treatment. The nanocomposites were added to the cell with various concentration, and incubated for 48 h. The cells were added into cold trichloroacetic acid solution (50 %, w/v) for 1–3 h, washed, and stained with SRB (0.2%, w/v) for 20 min. An ELISA plate reader (Synergy HT, Biotek Instruments) was used to determine absorption intensity at peaks of 492 nm and 620 nm. The percentage of growth inhibition (%) was calculated via Eq. (9) at a concentration of 100 µg/mL.

$$\text{Inhibition } \% = \frac{OD_c - OD_t}{OD_c} \times 100 \quad (9)$$

Where OD_c and OD_t are the optical density of the negative control and test samples, respectively.

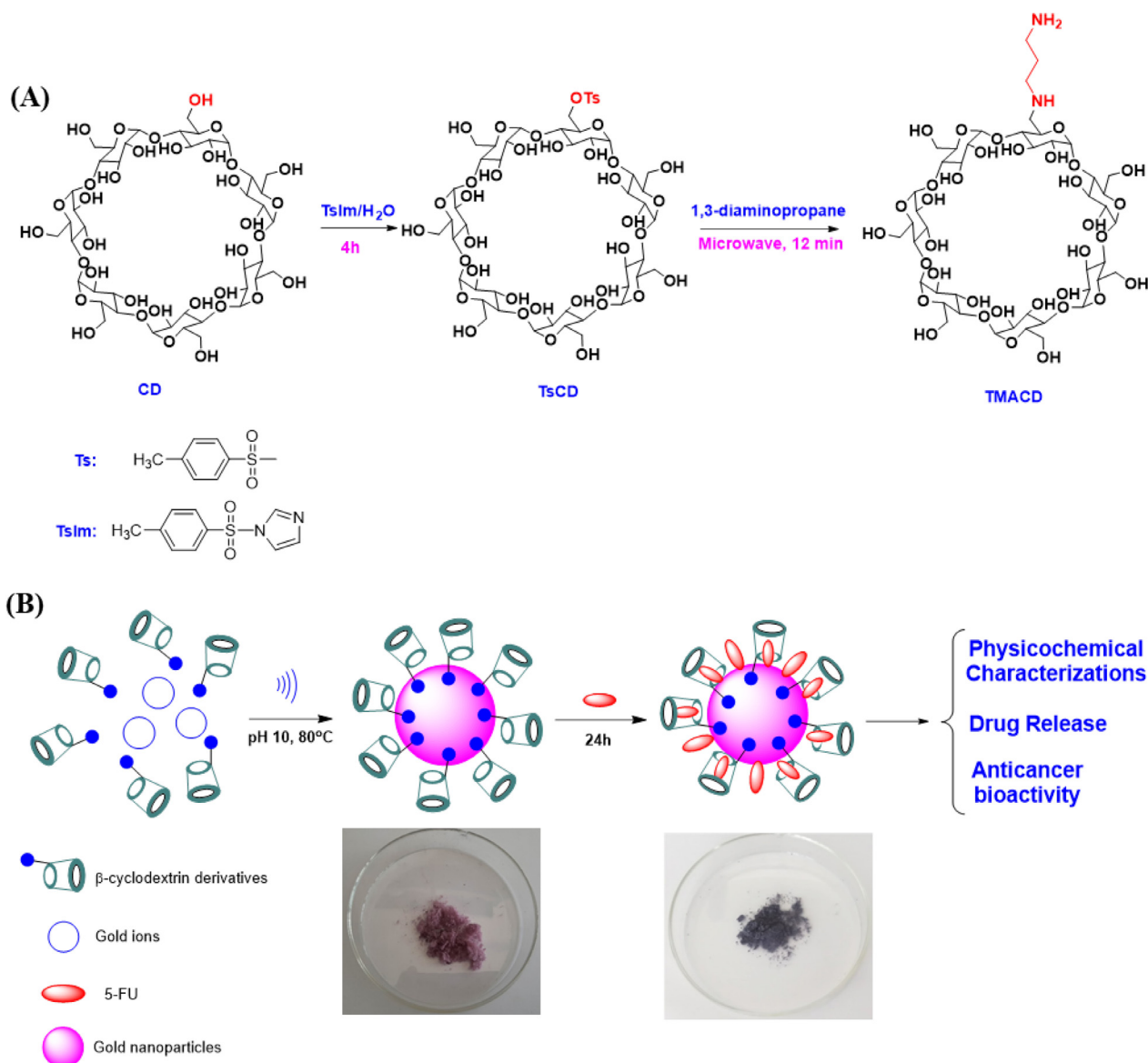
For determination of IC_{50} values which are identified as half maximal inhibitory concentration, the samples were performed at various concentrations and determined graphically using a curve-fitting algorithm. All values are expressed as means \pm standard deviation (SD) at least three independent experiments. Statistical analysis of the data was performed via Duncan's Multiple Range Test (DMRT) software package. All significant differences in a parameter were calculated by means of the paired Student's t -test with 95% ($P < 0.05$) confidence level.

3. Results and discussion

3.1. Synthesis of nanocomposite

Cyclodextrin-based carriers in combination with AuNPs have demonstrated effective drug delivery capabilities. Functionalizing cyclodextrin derivatives with specific functional groups, such as amines, can enhance the stability of nanocomposites (AuNPs/CDs) and improve their interaction with drug molecules. In the present work, various derivatives of β -cyclodextrin including β -CD, HPCD, and TMACD were employed. The TMACD derivative was synthesized via a 2-step process under ultrasound assistance (Scheme 1) (Shinde et al., 2018). β -CD reacted with 1-tosyl-1H-imidazole (TsIm) formed from tosyl chloride and imidazole, to afford mono-6-(p-toluensulfonyl)-6-deoxy- β -cyclodextrin (TsCD) which was then refluxed in 1,3-diaminopropane under microwave irradiation (300 W) for 12 min to obtain TMACD with total yield of 24.4 %. The structure of the synthesized products was well identified by QTOF-MS and NMR. The presence of protons in the range of 3.09 – 1.68 ppm in ¹H NMR spectrum is assigned to the group of 1,3-trimethylenediamine in the product TMACD (Shinde et al., 2018). Additionally, the value of the molecular mass in the QTOF-MS spectrum showed that TMACD possesses only one group of 1,3-trimethylenediamine. The synthesized derivatives (TsCD and TMACD) with high purity (>99%) were determined using HPLC spectra (Figure S2).

The influence of various functional groups of CD derivatives on the drug loading efficiency of nanocomposite AuNPs/CDs were illustrated in Scheme 1B. The blank nanocomposite AuNPs/CDs has easily fabricated under ultrasound assistance as a recent report (Nguyen et al., 2022). A similar procedure used for the fabrication of all nanocompos-



Scheme 1 Synthetic route of mono-6-(1,3-trimethylenediamine)-6-deoxy- β -cyclodextrin via two steps (A); study scheme and proposed formation mechanism for the synthesis of nanocomposites loading 5-FU (B).

ites was carried out under ultrasound irradiation at pH 10, 80 °C and 30 min. In contrast to the easy process of 5-FU encapsulation into β -CD in the solid state, the 5FU encapsulation efficiency in the aqueous solution is low due to the stability of the complexes (Jin et al., 2010, Di Donato et al., 2016, Melnikova et al., 2020). In addition, CDs are well known as good cryoprotectants of the freeze-dried process applied frequently for pharmaceutical fields (Vega et al., 2012, Zaghloul et al., 2022). Thus, in this work the blank nanocomposite solution was lyophilized after washing process. Then, anticancer drug 5-FU was loaded onto the blank nanocomposite using a stirring process for 24 h. The mixture was centrifuged and lyophilized for 8 h. The drug loaded nanocomposites, 5-FU@AuNPs/CDs were then checked the *in vitro* drug release kinetic and bioactivity of the drug loaded nanocomposites.

The color of products before and after the freeze-dried process were not changed, confirming that CDs well stabilized the

nanoparticles. However, significant changes in absorption spectra was recognized with the presence of 5-FU drug. The blank pink solid nanocomposites were obtained with absorption peaks at around 525 nm in UV-Vis spectra while 5-FU@AuNPs/CDs were blue solids with broad wavelengths at around 550 nm (Fig. 1A and 1B). The redshift of absorption peaks in the drug-loaded nanocomposites indicates significant change in morphology of the AuNPs in the presence of 5-FU. It may relate to the adsorption of 5-FU onto the surface of nanoparticles or induce competition between 5-FU/CDs complexes and CDs molecule in interaction with surface of nanoparticles. Importantly, UV-Vis spectra of the drug loaded nanocomposites clearly showed absorption peaks of 5-FU at around 266 nm, confirming successfully loaded drug onto the nanocomposite.

The effect of CD molecules on drug association efficiency (AE) and drug loading efficiency (LE) is described in

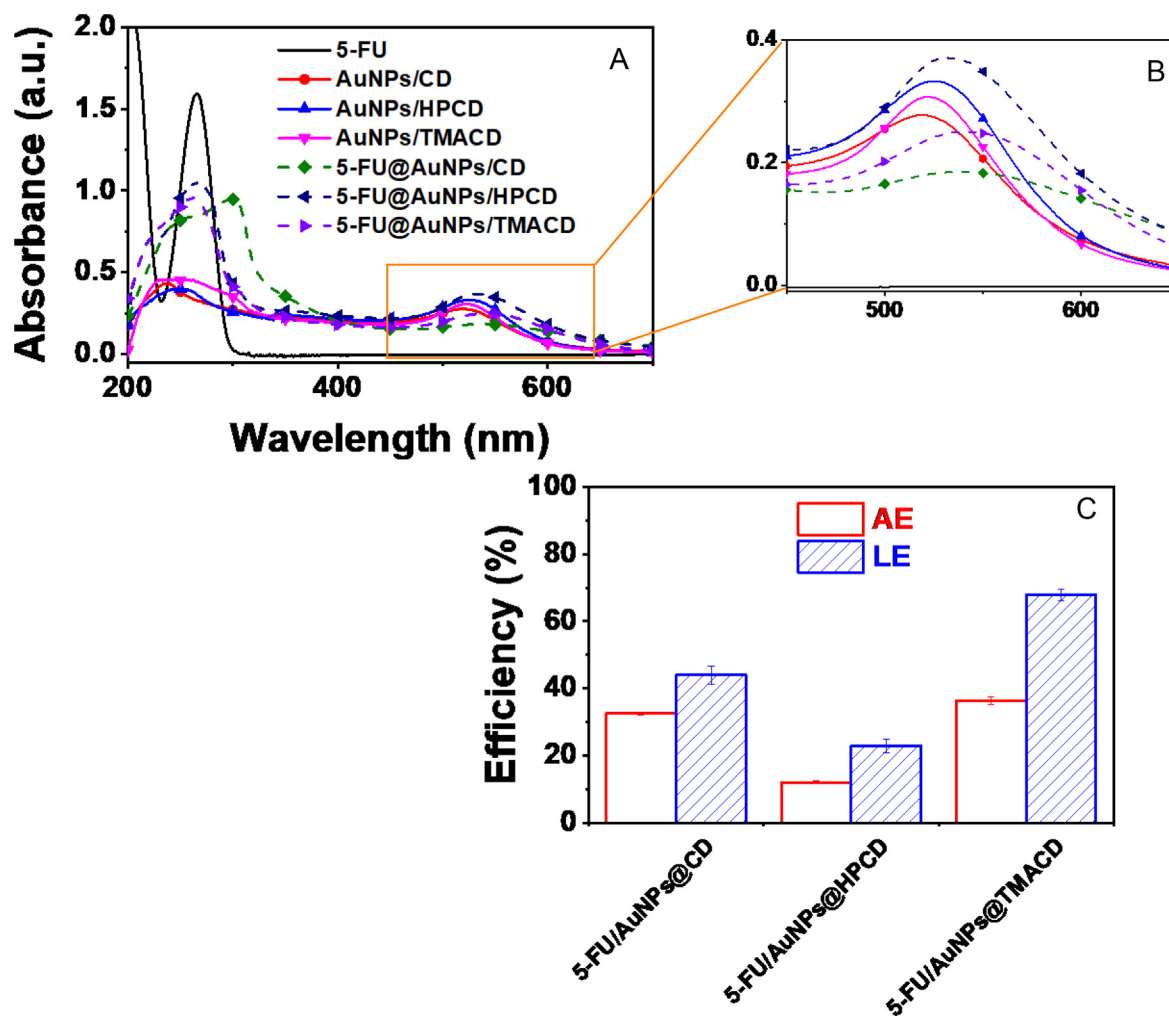


Fig. 1 UV-Vis spectra of 5-FU, blank nanocomposites and 5-FU-loaded nanocomposites presented in 200 – 700 nm (A) and 450 – 650 nm (B); and plots of association efficiency (AE) and loading efficiency (LE) of the drug from different nanocomposites (C).

Fig. 1B. The AE and LE of 5FU@AuNPs/CD were $32.5 \pm 0.5\%$ and $44.0 \pm 2.6\%$, respectively which were lower than 5-FU@AuNPs/TMACD ($36.3 \pm 1.2\%$ and $67.9 \pm 1.7\%$, respectively) while they were significantly higher than 5-FU@AuNPs/HPCD ($12.0 \pm 0.5\%$ and $22.9 \pm 2\%$, respectively). After centrifugation of 5-FU@AuNPs/HPCD, the supernatant remained dark red which showed the remnant of the high concentration of the nanocomposite. It is likely due to high solubility of HPCD in aqueous solution. However, the AuNPs/TMACD could encapsulate more drugs due to the better interaction between amine group of TMACD and AuNPs. Thus, encapsulation of 5-FU is strongly dependent on the functional groups of CD molecule.

3.2. Analysis of molecular interactions between 5-FU and β -cyclodextrins

The molecular interactions between 5-FU and CD molecules were investigated by computational analysis using *in silico* docking method (Aghaee et al., 2022). The ligand 5-FU was docked to CD structures to determine the physical parameters including affinity energy, inhibition constant and bond length.

The result is displayed in Fig. 2 and the most significant ligand interactions are listed in Table 1. The results in dock.dlg file based on Autodock package and built model by DSC suggested that the interactions of 5-FU with CD molecules are dependent on chemical structures of CD molecules. Three optimal poses in each model (500 run times) including pose 244, pose 71 and pose 60 were the most stable ligand conformation of 5-FU anchored to CD, HPCD and TMACD, respectively.

As seen in Fig. 2A, a pose 244 anchored to CD with the values of affinity energy and inhibition constant was found to be $-2.89 \text{ kcal.mol}^{-1}$ and 7.63 mM , respectively. The pose 244 formed two hydrogen bonds from oxygen atom of ketone group to hydrogen atom of hydroxyl benzyl group, $-\text{CH}_2-\text{OH}$ and another one, from hydrogen atom of N-H group in the pose to oxygen atom of the CD receptor. Meanwhile, the data showed that the parameters of pose 60 linked to TMACD is significantly higher than that of pose 244 interacted with CD molecule. The values of the affinity energy and inhibition constant for the interaction of pose 60 with TMACD were determined $-2.99 \text{ Kcal.mol}^{-1}$ and 6.42 mM , respectively while three hydrogen bonds linked from two oxygen atoms of two

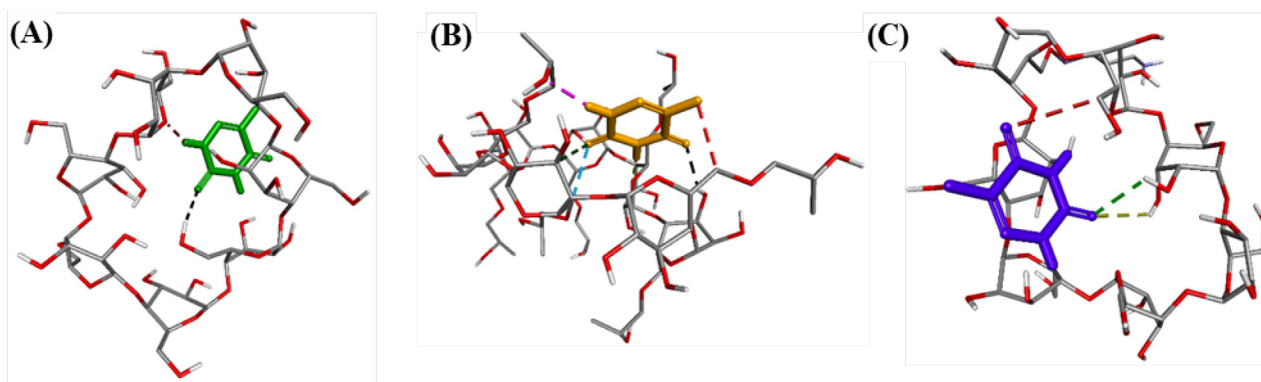


Fig. 2 The hydrogen bonds formed from the most stable conformations of compound 5-FU, ranked pose 244 to CD (A); pose 71 to HPCD (B); pose 60 to TMACD (C).

Receptor	Active pose	Affinity energy ^a	K _i ^b	Hydrogen bonding ^c	The property and bond length ^d
CD	Pose 244	-2.89	7.63	2	CD: H – Pose 244: O (2.78 Å) Pose 244: H – CD: O (2.17 Å)
HPCD	Pose 71	-3.24	4.25	6	HPCD: H – Pose 71: O (2.32 Å) Pose 71: H – HPCD: O (2.17 Å) Pose 71: H – HPCD: O (2.05 Å) HPCD: C – Pose 71: F (2.92 Å) HPCD: C – Pose 71: O (2.99 Å) HPCD: C – Pose 71: O (2.81 Å)
TMACD	Pose 60	-2.99	6.42	3	TMACD: H – Pose 60: O (2.60 Å) TMACD: H – Pose 60: O (2.84 Å) TMACD: C – Pose 60: O (3.40 Å)

^a Autodock package, kcal.mol⁻¹ unit in dock.dlg file; ^b Autodock package in dock.dlg file, mM unit; ^c Discovery Studio 2021 Client software (DSC); ^d Discovery Studio 2021 Client software (DSC).

ketone groups of this pose to two hydrogen atoms of alcohol groups, and one carbon atom of benzyl group on TMACD. However, the pose 60 interacted with TMACD was weaker than that of pose 71 with HPCD in both thermodynamic and ligand interactions. Indeed, the interaction of pose 71 with HPCD showed the affinity energy of -3.24 kcal.mol⁻¹ and inhibition constant of 4.25 mM while this pose formed six hydrogen bonds with HPCD molecule. Among them, the hydrogen bond formed from the hydrogen atom of pose 71 to oxygen atom of HPCD target was the strongest due to the shortest bonding length (2.05 Å) at pose 71: H - HPCD: O. The pose 71 was the best one in both thermodynamic and ligand interactions when 5-FU linked to various cyclodextrin derivatives. The atoms of pose 71 was relative to hydrogen bonds including hydrogen atoms of N-H group, oxygen atoms of carbonyl groups, and fluorine atom of C-F bond. Therefore, the interaction ability of the most stable conformation or ranked pose of drug 5-FU was determined to be in order of (pose 71 and HPCD) > (pose 60 and TMACD) > (pose 244 and CD). Interestingly, inconsistency between the interaction ability of 5-FU to CD derivatives in the computational data and the values of LE and AE in the corresponding nanocomposites confirmed that in addition to binding to CD molecules, 5-FU was also adsorbed onto AuNPs surface with significant changes of SPR peaks in drug loaded samples (Fig. 1).

3.3. Physicochemical characterization of the nanocomposite

Zeta potential and particle size in aqueous solution are principal criteria for evaluating nanostructure stability in the circulatory. Zeta potential and particle size distribution of the 5-FU loaded nanocomposites are described in Fig. 3A and 3B. All blank nanocomposites showed high negative surface charge in range of -49.4 mV to -85.7 mV that induces repulsion between nanoparticles, greatly reducing the propensity for aggregating and making high stability of the blank nanocomposites in aqueous solution (Figure S1). The result indicated that the nanocomposite based on AuNPs and CD molecules would be ideal for drug delivery. The drug loaded nanocomposites showed slight changes in zeta potentials (-38 mV to -60.6 mV) which were attributed to the presence of 5-FU in the nanocomposites (Fig. 3A). The high negative charge confirmed the stable drug loaded nanocomposites in aqueous solution, led to that drug was protected from degradation and unwanted binding.

Particle size of the blank nanocomposite is distributed in range of 1 – 1000 nm (Figure S1). However, the samples, AuNPs/CD and AuNPs/HPCD possess much lower average particle size (13 nm and 16 nm, respectively) than that of AuNPs/TMACD (105 nm). It is likely due to the attribution of the high steric ability of TMACD molecule to induce lower particle distribution in aqueous solution. Meanwhile, the par-

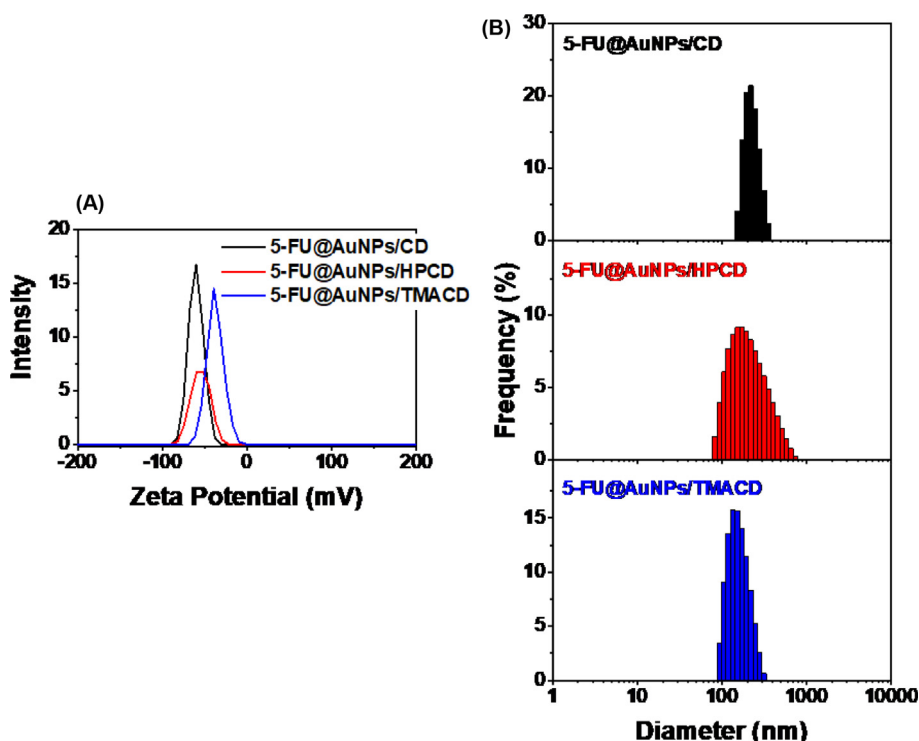


Fig. 3 Zeta potential (A) and dynamic light scattering (B) of drug loaded nanocomposites.

ticle size distribution of the drug loaded nanocomposites were significantly changed in comparison with the blank nanocomposites (80 – 1000 nm). Two samples, 5-FU@AuNPs/CD and 5-FU@AuNPs/TMACD have narrow distributions in range of 150 – 355 nm with a mean size of 213 ± 44.5 nm (PI of 0.427) and 93 – 313 nm with a mean size of 151 ± 43.5 nm (PI of 0.335), respectively whereas 5-FU@AuNPs/HPCD has a broad size range of 82 – 740 nm with a mean size of $212.7 \text{ nm} \pm 113.1 \text{ nm}$ (PI of 0.487) (Fig. 3B). High mean particle size and the high PDI of the drug loaded nanocomposites may relate to the loading of 5-FU into cyclodextrin cavity. Therefore, it reduced nanoparticles stability and induced aggregation of particles.

The crystalline structure of 5-FU, the blank and drug loaded nanocomposites were evaluated by PXRD patterns as shown in Fig. 4A. The PXRD patterns of the blank nanocomposites showed feature peaks of AuNPs crystal at 2θ angles of 38.4° , 44.8° , 64.4° and 77.5° , assigning to the face-centred cubic (fcc) of (111), (200), (220) and (311), respectively (card number 00-004-0783) (Nguyen et al., 2021). The PXRD pattern of 5-FU drug showed crystalline structure with a strongly intensive peak at 2θ angle of 28.4° which consisted with the previous report (Arafat et al., 2020). The PXRD data of the drug loaded nanocomposites indicated characteristic peaks of both 5-FU drug and AuNPs/CDs nanocomposite. Moreover, the peak intensity at 2θ angle of 28.4° was in order of 5-FU@AuNPs/TMACD > 5-FU@AuNPs/CD > 5-FU@AuNPs/HPCD which were related to the content of 5-FU drug in the samples. The result was consistent with the loading efficiency values of the drug loaded nanocomposites (Fig. 1C).

The FTIR spectra of 5-FU, blank and drug loaded nanocomposites were displayed in Fig. 4B. The FTIR spectra of the blank nanocomposites showed the similar absorption peaks of glucose molecules in CD which appeared at peaks

around 3420 , 2940 , 1640 , 1414 and 1031 cm^{-1} . The peaks at 3420 cm^{-1} and 1414 cm^{-1} were the stretching and bending vibrations of OH groups, respectively. The peak at 2940 cm^{-1} was the alkyl C-H stretching vibrations of glucose molecules. The peak at 1640 cm^{-1} related to the stretching vibration of the C - C groups and peak at 1030 cm^{-1} corresponded to the stretching vibration of C-O groups. The results confirmed that all CD derivatives effectively stabilised AuNPs. Comparing the previous report, the AuNPs/CD spectrum showed the disappearance of peak at 1704 cm^{-1} (characteristic of COO^- group), indicating that the compounds bearing carboxyl groups might be removed from washing process *via* the dialysis bag. The spectrum of 5-FU drug indicated feature peaks at 3151 cm^{-1} and $2934\text{--}2832 \text{ cm}^{-1}$ due to the N-H and C-H stretching vibrations, respectively. The peaks at $1769\text{--}1662 \text{ cm}^{-1}$ were to the C = O stretch models; the peaks at 1350 and 1248 cm^{-1} were of vibrational models of C-N and C-F groups, respectively (Melnikova et al., 2020). The FTIR spectra of drug loaded nanocomposites showed all feature peaks of both the blank nanocomposites (1414 and 1034 cm^{-1}) and 5-FU drug (1722 , 1350 and 1248 cm^{-1}) which confirmed the presence of drug in the nanocomposites. The results proved that the 5-FU drug was successfully encapsulated into the carrier AuNPs/CDs.

For study on thermal stability, thermogravimetric analysis of 5-FU, the blank and drug loaded nanocomposites was investigated in the air atmosphere with a heating rate of $10 \text{ }^\circ\text{C}/\text{min}$ as shown in Fig. 5 and listed in Table S1. TGA curve of drug 5-FU showed completely thermal decomposition within only one stage between 273 and $318 \text{ }^\circ\text{C}$ (98.5%), confirming high purity of drug. The blank nanocomposites exhibited the different thermal properties. Thermal decomposition of AuNPs/HPCD occurred in one stage of $258\text{--}540 \text{ }^\circ\text{C}$ (78.6%) while the samples, AuNPs/CD and AuNPs/TMACD

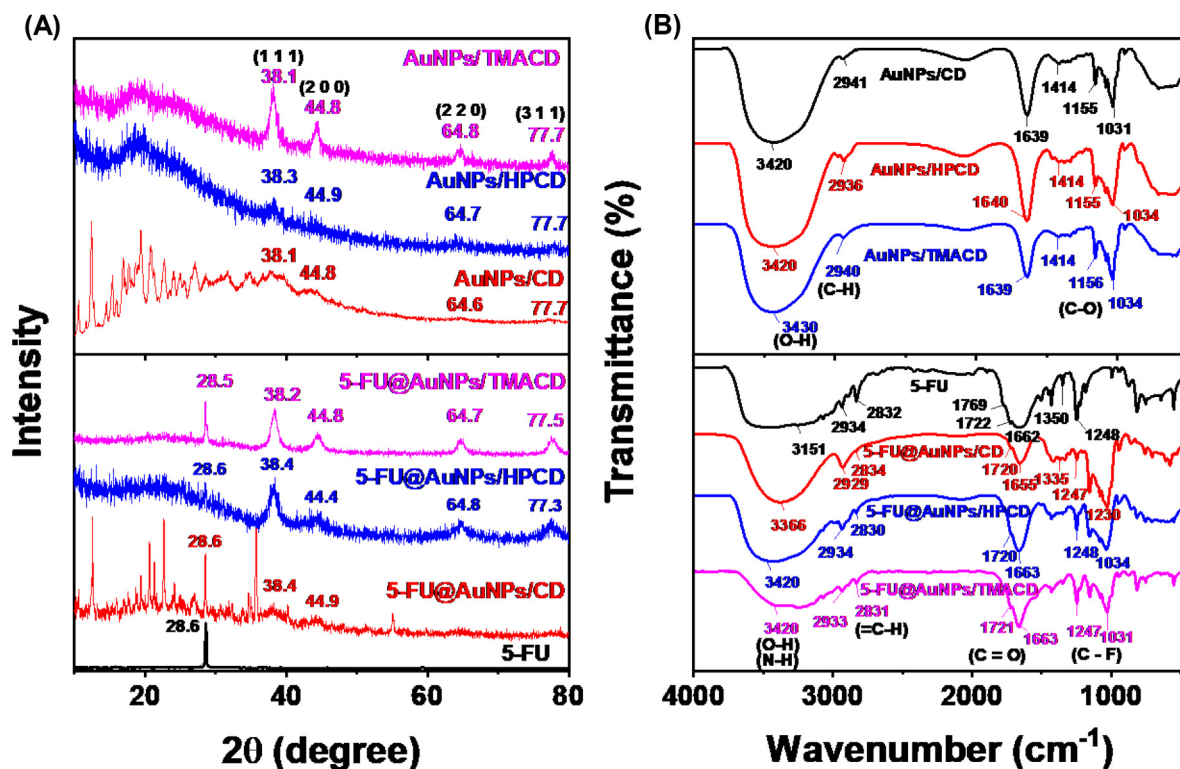


Fig. 4 PXRD patterns (A); FTIR spectra of 5-FU, blank nanocomposites, and drug loaded nanocomposites.

showed the decomposition behavior in three stages. The first step relates to evaporation of moisture which occurs at 30 – 100 °C with mass loss of 2.3 % and 2.7%, respectively. The second step mainly occurs at 100 – 530 °C with mass loss of 73.8% and 65.5%, respectively which corresponds to oxidation of glucose molecules in oligosaccharide chains. The last step is determined between 530 and 790 °C with mass loss of 4.3% and 5.1%, respectively. Whilst the drug loaded nanocomposites exhibited significant difference compared to the blank samples. All drug loaded samples showed thermal decomposition via three stages with various mass loss including moisture evaporation (30 – 100 °C) with mass loss of 2.3 – 7.4%, oxidation of saccharide molecules (100 – 530 °C) with mass loss of 52.7 – 77.4% and carbonation (530 – 790 °C) with mass loss of 4.1 – 14.1 %. The significant difference in mass loss among the drug loaded nanocomposites might be attributed to the different ratios of organic compounds including drug and saccharide molecules in the samples which is agreement with loading efficiency values of the nanocomposites (Fig. 1C).

The SEM and TEM images of the blank and drug loaded nanocomposites were investigated to evaluate the effect of loading drug as well as various CDs on their morphologies and particle size (Fig. 6). The SEM images indicated that there were no significant changes of morphology among CD derivatives, however, the difference was observed clearly between the blank nanocomposite and the drug loaded nanocomposite. Indeed, the blank nanocomposites showed very smooth surfaces (seen in Fig. 6A1, 6C1 and 6E1) whereas the surface of the drug load composites was very rough (seen in Fig. 6B1, 6D1 and 6F1). It is likely because the presence of drug in sample induced softer structure of the drug loaded nanocomposite.

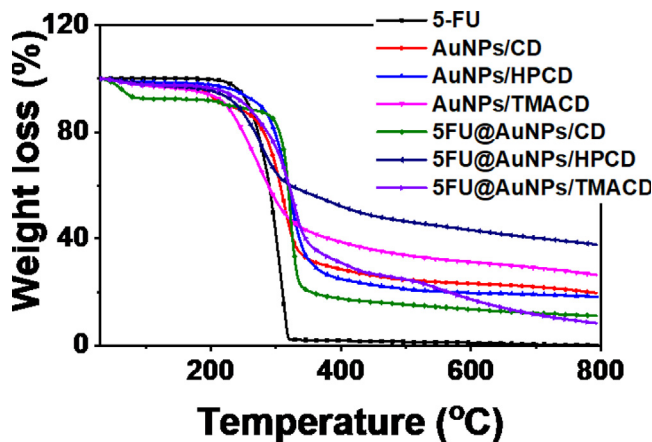


Fig. 5 TGA curves of 5-FU, blank nanocomposites, and drug loaded nanocomposites.

TEM images showed that AuNPs in all samples existed mostly spherical shapes with slightly different size distributions. The samples AuNPs/CD and AuNPs/TMACD exhibited the broad distribution of size in range of 3 – 18 nm with the highest distribution frequency of 12 nm and 3 – 12 nm with the highest distribution frequency of 9 nm while the size distribution of AuNPs/HPCD was in narrow range of 9–15 nm with the highest distribution frequency of 12 nm. Also, the drug loaded nanocomposites are observed in a similar trend with size distribution of AuNPs stabilized by different CD molecules. 5-FU@AuNPs/CD showed range of 4 – 13 nm with the highest distribution frequency of 8 nm and 5-FU@AuNPs/TMACD showed a broad range of 4 – 15 nm with the highest

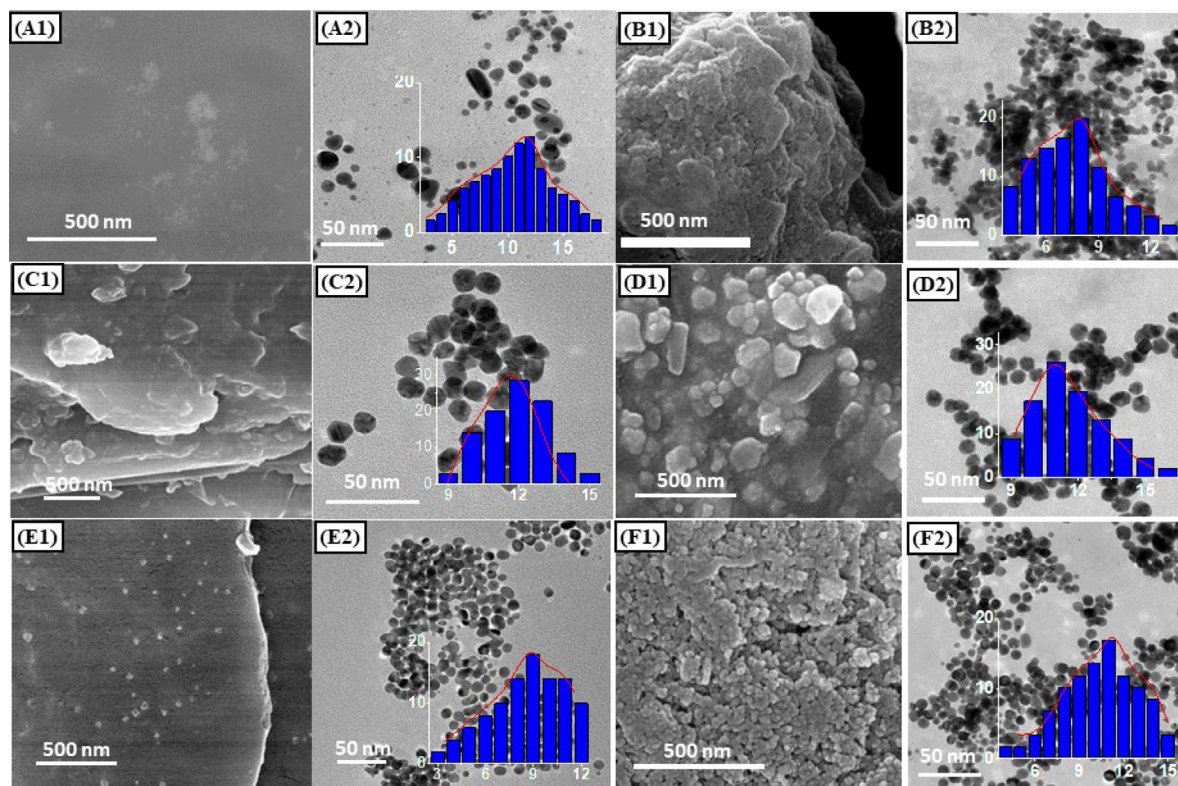


Fig. 6 SEM, TEM images and size distribution (in set) of nanocomposites: AuNPs/CD (A1 and A2), 5-FU@AuNPs/CD (B1 and B2), AuNPs/HPCD (C1 and C2), 5-FU@AuNPs/HPCD (D1 and D2), 5-FU@AuNPs/DAPCD (E1 and E2), and 5-FU@AuNPs/TMACD (F1 and F2).

distribution frequency of 11 nm. Size of 5-FU@AuNPs/HPCD is distributed in range of 9 – 16 nm with the highest distribution frequency of 11 nm. Notably, the TEM images of the blank nanocomposites indicated separable distribution between the nanoparticles whereas the drug loaded nanocomposites showed the significant aggregation of nanoparticles. The drug 5-FU induced the significant change in surface plasmonic resonance (SPR) of AuNPs, consistent with red shift data in UV-Vis spectra (Fig. 1A).

3.4. *In vitro* drug release profile

The drug 5-FU is mainly administered *via* intravenous injection for the cancers therapy or applied on the skin in the creamy form (Khan et al., 2022). Thus, in the experiment, the *in vitro* release profile of drug 5-FU was performed in PBS at pH 7.4. The release data of the nanocomposites, 5-FU@AuNPs/CD, 5-FU@AuNPs/HPCD and 5-FU@AuNPs/TMACD compared with the free drug suspension was presented in Fig. 7A. The drug loaded nanocomposites showed a sustained release behaviour followed by a nonlinear profile. The released drug of 5-FU@AuNPs/CD, 5-FU@AuNPs/HPCD and 5-FU@AuNPs/TMACD after 24 h was found to be $29.45 \pm 0.98 \%$, $23.13 \pm 2.29 \%$ and $25.28 \pm 1.46 \%$, respectively. The slight difference among CD derivatives showed the effect of functional groups on the protection of drug in the nanocomposites. Conversely, the free 5-FU suspension exhibited a relatively fast release, achieving up to $92.01 \pm 4.51\%$ after only 5 h. The release profile of

the nanocomposites suggested that within an hour, drug released was fast, then it was slow down for 24 h indicating a biphasic behavior of the AuNPs-based nanocomposites (England et al., 2015). When comparing to the previous study on the release behavior of cyclodextrin complexes (Jin et al., 2010, Mashaqbeh et al., 2022), our nanocomposites were more stable. The high stability was attributed to the interaction between drug and plasmonic surface of AuNPs which obstructed the diffusion of drug into the solution. Therefore, the drug was well protected in the particles during the delivery process.

For proving the release mechanism of NPs, the kinetic study of drug 5-FU from various nanocomposites was simply determined by using graphical representation methods including zero order, first order, Hixson-Crowell, Higuchi and Korsmeyer-Peppas (Siepmann and Siepmann 2008). The correlation values of release parameters (R^2) from fitting the release profiles are listed in Table 2. According to correlation coefficients, the release data of the nanocomposites well fitted to Korsmeyer-Peppas model with $R^2 > 0.98$. For the Korsmeyer-Peppas release model, exponent value (n) lower than 0.5 confirmed the Fickian diffusion mechanism which describe how drug released from matrix of nanocomposites. In this model, the solvent diffusion is faster than relaxation of CD molecules and the kinetics of the phenomenon can be characterized by the diffusivity. Fig. 5A showed an initial burst from the nanocomposites in the first 1 h of dissolution which occurs in significant percentage of the drug released during the early stage of the release process and then followed by a

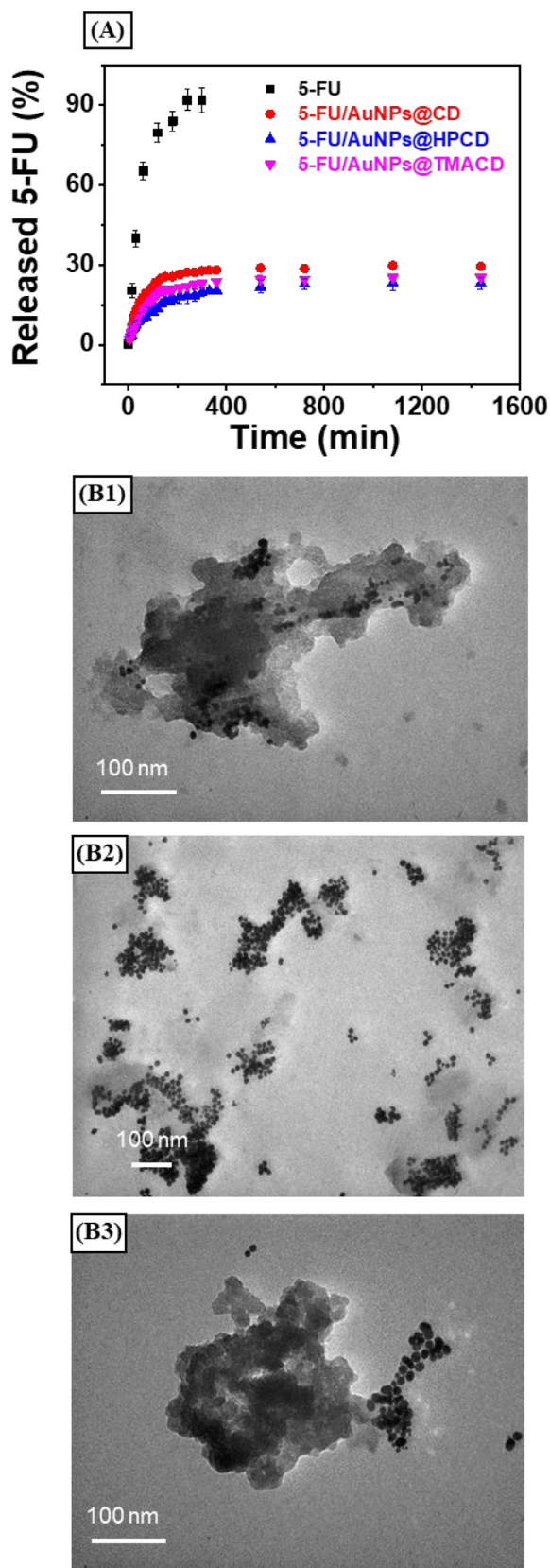


Fig. 7 Drug release profile of the drug loaded nanocomposites at pH 7.4 (A) and TEM images of the 5-FU@AuNPs/CD (B1), 5-FU@AuNPs/HPCD (B2) and 5-FU@AuNPs/TMACD (B3) recovered after 24 h at pH 7.4.

slow release to tend to the asymptote of saturation concentration of the drug. The result confirmed good drug protection of hydroxyl and amino alkyl groups from solvent diffusion.

To better understand the release behavior, the drug loaded nanocomposites were recovered after release and further characterized by TEM as presenting in Fig. 7B1-7B3. The AuNPs were aggregated and the formation of organic float enveloping AuNPs after 24 h of the release process was observed. The organic float was the swelling of the cyclic macromolecules in the release medium which induced the aggregation of particles (Nguyen et al., 2022). The obtained result is consistent with the kinetic data.

3.5. Cytotoxicity assay

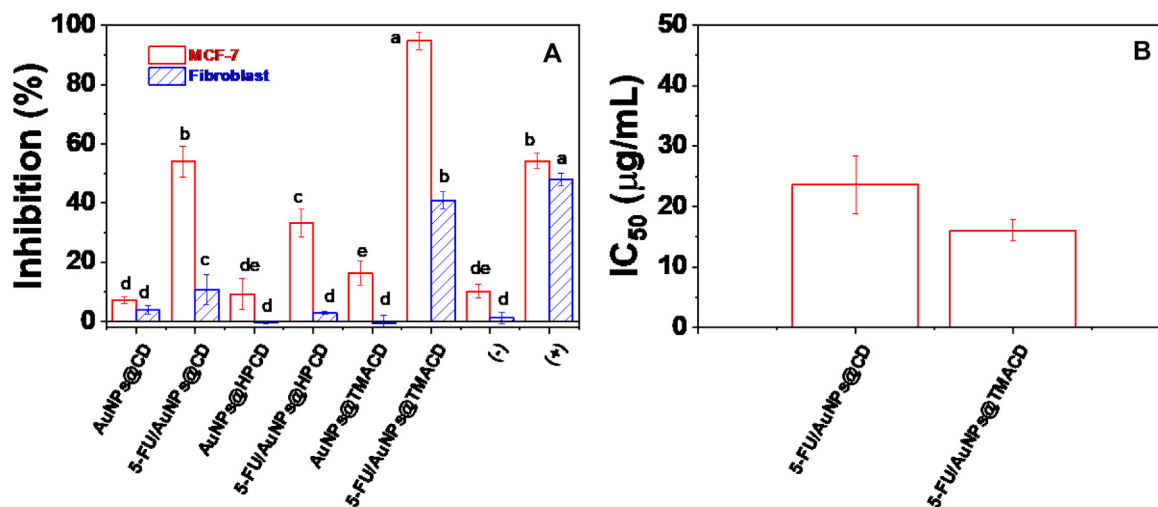
The cytotoxic activity of the blank nanocomposites and the drug loaded nanocomposites was evaluated on breast cancer cells (MCF-7) and normal cells (fibroblast) using a MTT assay method. Fig. 8A showed the toxicity of nanocomposites against both cell lines at a concentration of 100 $\mu\text{g}/\text{mL}$. The values higher than 50% were selected to determine the IC_{50} (Fig. 8B). As seen in Fig. 8A, all blank nanocomposites exhibited no toxicity effect against both normal and cancer cells. The result suggests high biocompatibility of materials based on AuNPs and CDs. Meanwhile, the drug loaded nanocomposites showed the different bioactivity against cell lines which was dependent on CD structures. The 5-FU@AuNPs/HPCD exhibited the low anticancer bioactivity ($33.42 \pm 4.73\%$) and no effect against normal cells. The 5-FU@AuNPs/CD showed high inhibition against cancer cells ($54.00 \pm 5.21\%$) but no activity against normal cells while 5-FU@AuNPs/TMACD gave strong toxicity against cancer cells ($94.76 \pm 2.87\%$) and low toxicity against for fibroblast ($40.92 \pm 2.89\%$). The result showed that the bioactivity of 5-FU@AuNPs/CD against MCF-7 cells ($\text{IC}_{50} = 23.66 \pm 4.76 \mu\text{g}/\text{mL}$) was slightly lower than the bioactivity of 5-FU@AuNPs/TMACD ($\text{IC}_{50} = 16.04 \pm 1.76 \mu\text{g}/\text{mL}$). It is clear that amine group in CD molecule significantly enhanced toxicity of 5-FU against cells MCF-7. High anticancer activity of both nanocomposites 5-FU@AuNPs/CD and 5-FU@AuNPs/TMACD is attributed to great LE values of 5-FU. Hence, the formation of complexes between drug and AuNPs/CDs can increase toxicity of the drug when the drug interacts with cells. Moreover, the nanocomposites 5-FU@AuNPs/CDs in this work revealed the higher anticancer efficiency against MCF-7 than the other AuNPs-based nanocomposites reported in the literature (Table 3). It suggests that the nanocomposites AuNPs/CD and AuNPs/TMACD should be used as potential 5-FU drug delivery system for the treatment and therapy of breast cancer.

4. Conclusion

Metal nanoparticle-oligosaccharide hybrid materials were obtained from modified β -cyclodextrins and gold nanoparticles as effective carriers for anticancer drug via the ultrasound-assisted synthesis. FTIR spectra and powder XRD patterns indicated successful intercalation of 5-FU into AuNPs/CDs. UV-Vis spectroscopy and TEM images showed the changes in AuNPs surface when 5-FU was included into the nanocomposites which possessed the average size of 8–11 nm. The loading capacity showed the nanocomposite of TMACD derivative having the highest associate efficiency and loading efficiency of the drug. The docking model between 5-FU and cyclodextrin mole-

Table 2 Release drug kinetic data of different nanocomposites.

Kinetic models	5-FU@AuNPs/CD			5-FU@AuNPs/HPCD			5-FU@AuNPs/TMACD		
	Constant (x10 ⁻³)	n	R ²	Constant (x10 ⁻³)	n	R ²	Constant (x10 ⁻³)	n	R ²
Zero order	41.0 ± 10.4	–	0.30	57.4 ± 9.4	–	0.52	27.9 ± 3.9	–	0.59
First order	0.58 ± 0.14	–	0.32	0.77 ± 0.11	–	0.57	0.41 ± 0.05	–	0.63
Hixson-Crowell	13.6 ± 3.4	–	0.29	19.1 ± 3.1	–	0.52	9.2 ± 1.3	–	0.59
Hugichi	1632 ± 167	–	0.74	1348 ± 69	–	0.91	860 ± 85	–	0.75
Korsmeyer-Peppas	1115 ± 5.9	0.070 ± 0.002	0.98	1030 ± 5.5	0.040 ± 0.002	0.95	1094 ± 13.4	0.073 ± 0.002	0.97

**Fig. 8** Inhibition (A) and IC₅₀ values (B) of drug, blank nanocomposites and drug loaded nanocomposites against cancer cells MCF-7 and normal cell fibroblast. Different letters indicate significant differences at p < 0.05.**Table 3** AuNPs-based nanocomposite loading 5-FU drug for treatment of cell line MCF-7.

Name	Particle Size (nm)	LE or/and AE (%)	Cytotoxicity against MCF-7	Ref.
AuNPs/Chitosan	5	LE = 41.0	IC ₅₀ = 31.2 µg/ml	(Nivethaa et al., 2015)
AuNPs/Graphene oxide	10	–	Cell viability = 48% at 2.5 µg/mL	(Sanad et al., 2019)
AuNPs/Folated Chitosan	31–33	AE = 79.0	IC ₅₀ = 20 µg/mL	(Akinyelu and Singh 2019)
AuNPs/HPCD	19	–	IC ₅₀ = 100 µM	(Lakkakula et al., 2021)
AuNPs/Albumin	249	LE = 89.0 AE = 64.0	Cell viability = 18.09% at 100 µg/mL	(Mahdi et al., 2020)
AuNPs/CD	8–11	AE = 32.5 LE = 44.0	Cell viability = 54.00 % at 100 µg/mL IC ₅₀ = 23.66 µg/mL	This work
AuNPs/HPCD		AE = 12.0 LE = 22.9	Cell viability = 33.42 % at 100 µg/mL	
AuNPs/TMACD		AE = 36.3 LE = 67.9	Cell viability = 94.76 % at 100 µg/mL IC ₅₀ = 16.04 µg/mL	

cules showed that the best interaction of pose 71 and HPCD target at active atoms of 5-FU including hydrogen atoms of N–H groups, two oxygen of ketone groups and fluorine atom of C–F group. Furthermore, the *in vitro* release mechanism showed that the drug release via biphasic model with swelling of saccharide molecules in PBS. The release data indicated that our nanocomposites had good protection of 5-FU with a mean drug release from 23.13 – 29.45 %. The tox-

icity of the drug loaded nanocomposite showed the different bioactivity, depending on carriers. Both nanocomposites, 5-FU@AuNPs/CD and 5-FU@AuNPs/TMACD possessed the good toxic effect against MCF-7 and safety to the normal cells. The results showed that the 1,3-diaminopropane group significantly enhanced efficiency of loading drug and anticancer activity of the nanocomposite based on AuNPs and β -cyclodextrin.

Declaration of Competing Interest

The authors declare that they have no known competing financial interests or personal relationships that could have appeared to influence the work reported in this paper.

Acknowledgements.

The work is supported by Vietnam Academy of Science and Technology, Vietnam with numbers VAST03.02/20-21 and NCVCC15.01/22-23.

Appendix A. Supplementary material

The Supporting Information is available free of charge on website at DOI:..... scheme of docking experiment; additional data of DLS and zeta potential of blank samples; table of TGA data and copies of QTOF-MS, ¹H and ¹³C NMR spectra. Supplementary data to this article can be found online at <https://doi.org/10.1016/j.arabjc.2023.105079>.

References

- Aghae, M., Mohammadi, K., Hayati, P., et al, 2022. A novel 3D Ag (I) metal-organic coordination polymer (Ag-MOCP): Crystallography, Hirshfeld surface analysis, antibacterial effect and molecular docking studies. *J. Solid State Chem.* 310, 123013.
- Ajnai, G., Chiu, A., Kan, T., et al, 2014. Trends of gold nanoparticle-based drug delivery system in cancer therapy. *J. Experimental Clin. Med.* 6, 172–178.
- Akinyelu, J., Singh, M., 2019. Folate-tagged chitosan-functionalized gold nanoparticles for enhanced delivery of 5-fluorouracil to cancer cells. *Appl. Nanosci.* 9, 7–17.
- Akkin, S., Varan, G., Aksüt, D., et al, 2022. A different approach to immunochemotherapy for colon Cancer: Development of nanoplexes of cyclodextrins and Interleukin-2 loaded with 5-FU. *Int. J. Pharm.* 623, 121940.
- Ali, S., Chen, X., Shi, W., et al, 2021. Recent advances in silver and gold nanoparticles-based colorimetric sensors for heavy metal ions detection: a review. *Crit. Rev. Anal. Chem.*, 1–33
- Arafat, M., Fouladian, P., Wignall, A., et al, 2020. Development and in vitro evaluation of 5-fluorouracil-eluting stents for the treatment of colorectal cancer and cancer-related obstruction. *Pharmaceutics* 13, 17.
- Arockia Jency, D., Umadevi, M., Sathe, G., 2015. SERS detection of polychlorinated biphenyls using β -cyclodextrin functionalized gold nanoparticles on agriculture land soil. *J. Raman Spectrosc.* 46, 377–383.
- Bulut, O., Yilmaz, M.D., 2021. Catalytic evaluation of biocompatible chitosan-stabilized gold nanoparticles on oxidation of morin. *Carbohydr. Polym.* 258, 117699.
- Chen, Y., Feng, X., 2022. Gold nanoparticles for skin drug delivery. *Int. J. Pharm.* 122122
- Chen, X., Zhao, X., Wang, G., 2020. Review on marine carbohydrate-based gold nanoparticles represented by alginate and chitosan for biomedical application. *Carbohydr. Polym.* 244, 116311.
- Chowdhury, P., Nagesh, P.K., Hatami, E., et al, 2019. Tannic acid-inspired paclitaxel nanoparticles for enhanced anticancer effects in breast cancer cells. *J. Colloid Interface Sci.* 535, 133–148.
- Daraee, H., Eatemadi, A., Abbasi, E., et al, 2016. Application of gold nanoparticles in biomedical and drug delivery. *Artif. Cells Nanomed. Biotechnol.* 44, 410–422.
- Di Donato, C., Lavorgna, M., Fattorusso, R., et al, 2016. Alpha-and beta-cyclodextrin inclusion complexes with 5-fluorouracil: Characterization and cytotoxic activity evaluation. *Molecules* 21, 1644.
- Elahi, N., Kamali, M., Baghersad, M.H., 2018. Recent biomedical applications of gold nanoparticles: A review. *Talanta* 184, 537–556.
- El-Hachem, N., B. Haibe-Kains, A. Khalil, et al., 2017. AutoDock and AutoDockTools for protein-ligand docking: beta-site amyloid precursor protein cleaving enzyme 1 (BACE1) as a case study. *Neuroproteomics, Springer:* 391-403.
- England, C.G., Miller, M.C., Kuttan, A., et al, 2015. Release kinetics of paclitaxel and cisplatin from two and three layered gold nanoparticles. *Eur. J. Pharm. Biopharm.* 92, 120–129.
- Gu, X., Xu, Z., Gu, L., et al, 2021. Preparation and antibacterial properties of gold nanoparticles: A review. *Environ. Chem. Lett.* 19, 167–187.
- Heo, D.N., Yang, D.H., Moon, H.-J., et al, 2012. Gold nanoparticles surface-functionalized with paclitaxel drug and biotin receptor as theranostic agents for cancer therapy. *Biomaterials* 33, 856–866.
- Ho, T.-T.-T., Dang, C.-H., Huynh, T.-K.-C., et al, 2021. In situ synthesis of gold nanoparticles on novel nanocomposite lactose/alginate: Recyclable catalysis and colorimetric detection of Fe (III). *Carbohydr. Polym.* 251, 116998.
- Hu, Q.-D., Tang, G.-P., Chu, P.K., 2014. Cyclodextrin-based host-guest supramolecular nanoparticles for delivery: from design to applications. *Acc. Chem. Res.* 47, 2017–2025.
- Ielo, I., Rando, G., Giacobello, F., et al, 2021. Synthesis, chemical-physical characterization, and biomedical applications of functional gold nanoparticles: A review. *Molecules* 26, 5823.
- Jeong, E.H., Jung, G., Hong, C.A., et al, 2014. Gold nanoparticle (AuNP)-based drug delivery and molecular imaging for biomedical applications. *Arch. Pharm. Res.* 37, 53–59.
- Jin, L., Liu, Q., Sun, Z., et al, 2010. Preparation of 5-fluorouracil/ β -cyclodextrin complex intercalated in layered double hydroxide and the controlled drug release properties. *Ind. Eng. Chem. Res.* 49, 11176–11181.
- Khan, N.H., Mir, M., Qian, L., et al, 2022. Skin cancer biology and barriers to treatment: Recent applications of polymeric micro/nanostructures. *J. Adv. Res.* 36, 223–247.
- Kim, C.-K., Ghosh, P., Rotello, V.M., 2009. Multimodal drug delivery using gold nanoparticles. *Nanoscale* 1, 61–67.
- Kumar, A., Zhang, X., Liang, X.-J., 2013. Gold nanoparticles: emerging paradigm for targeted drug delivery system. *Biotechnol. Adv.* 31, 593–606.
- Lakkakula, J.R., Krause, R.W.M., Divakaran, D., et al, 2021. 5-Fu inclusion complex capped gold nanoparticles for breast cancer therapy. *J. Mol. Liq.* 341, 117262.
- Liu, Y., Male, K.B., Bouvrette, P., et al, 2003. Control of the size and distribution of gold nanoparticles by unmodified cyclodextrins. *Chem. Mater.* 15, 4172–4180.
- Lu, S., Wang, A., Ma, Y., et al, 2016. Cyclodextrin type dependent host-guest interaction mode with phthalocyanine and their influence on photodynamic activity to cancer. *Carbohydr. Polym.* 148, 236–242.
- Mahdi, W.A., Hussain, A., Ramzan, M., 2020. 5-Fluorouracil loaded biogenic and albumin capped gold nanoparticles using bacterial enzyme—in vitro-in silico Gastroplus® simulation and prediction. *Processes* 8, 1579.
- Mai, T.-C., Tran, N.-T., Mai, D.-T., et al, 2022. Supercritical CO₂ assisted extraction of essential oil and naringin from *Citrus grandis* peel: in vitro antimicrobial activity and docking study. *RSC Adv.* 12, 25962–25976.
- Male, K.B., Li, J., Bun, C.C., et al, 2008. Synthesis and stability of fluorescent gold nanoparticles by sodium borohydride in the presence of mono-6-deoxy-6-pyridinium- β -cyclodextrin chloride. *J. Phys. Chem. C* 112, 443–451.
- Mashaqbeh, H., Obaidat, R., Al-Shar'i, N.A., et al, 2022. Weak complexation of 5-fluorouracil with β -cyclodextrin, carbonate, and

- dianhydride crosslinked β -cyclodextrin: in vitro and in silico studies. *Res. Pharmaceut. Sci.* 17, 334.
- Melnikova, D.L., Badrieva, Z.F., Kostin, M.A., et al, 2020. On complex formation between 5-fluorouracil and β -cyclodextrin in solution and in the solid state: IR markers and detection of short-lived complexes by diffusion NMR. *Molecules* 25, 5706.
- Mohandoss, S., Edison, T.N.J.I., Atchudan, R., et al, 2020. Ultrasonic-assisted efficient synthesis of inclusion complexes of salsalate drug and β -cyclodextrin derivatives for potent biomedical applications. *J. Mol. Liq.* 319, 114358.
- Nejati, K., Dadashpour, M., Gharibi, T., et al, 2021. Biomedical applications of functionalized gold nanoparticles: a review. *J. Clust. Sci.*, 1–16
- Nguyen, C.-H., Banh, K.-S., Dang, C.-H., et al, 2022. β -cyclodextrin/alginate nanoparticles encapsulated 5-fluorouracil as an effective and safe anticancer drug delivery system. *Arab. J. Chem.* 15, 103814.
- Nguyen, C.-H., Banh, K.-S., Le, V.-D., et al, 2022. Ultrasound-assisted synthesis of gold nanoparticles supported on β -cyclodextrin for catalytic reduction of nitrophenols. *Inorg. Chem. Commun.* 145, 109979.
- Nguyen, C.-H., Banh, K.-S., Le, V.-D., et al, 2022. Ultrasound-assisted synthesis of gold nanoparticles supported on β -cyclodextrin for catalytic reduction of nitrophenols. *Inorg. Chem. Commun.* 109979
- Nguyen, T.-M.-T., Nguyen, T.-A.-T., Tuong-Van Pham, N., et al, 2021. Biosynthesis of metallic nanoparticles from waste *Passiflora edulis* peels for their antibacterial effect and catalytic activity. *Arab. J. Chem.* 14, 103096.
- Nguyen, T.-D., Vo, T.-T., Huynh, T.-T.-T., et al, 2019. Effect of capping methods on the morphology of silver nanoparticles: study on the media-induced release of silver from the nanocomposite β -cyclodextrin/alginate. *New J. Chem.* 43, 16841–16852.
- Nivethaa, E., Dhanavel, S., Narayanan, V., et al, 2015. An in vitro cytotoxicity study of 5-fluorouracil encapsulated chitosan/gold nanocomposites towards MCF-7 cells. *RSC Adv.* 5, 1024–1032.
- Özkahraman, B., Acar, I., Güçlü, G., 2023. Synthesis of N-vinylcaprolactam and methacrylic acid based hydrogels and investigation of drug release characteristics. *Polym. Bull.* 80, 5149–5181.
- Park, C., Youn, H., Kim, H., et al, 2009. Cyclodextrin-covered gold nanoparticles for targeted delivery of an anti-cancer drug. *J. Mater. Chem.* 19, 2310–2315.
- Rezk, A.I., Obiweluozor, F.O., Choukrani, G., et al, 2019. Drug release and kinetic models of anticancer drug (BTZ) from a pH-responsive alginate polydopamine hydrogel: Towards cancer chemotherapy. *Int. J. Biol. Macromol.* 141, 388–400.
- Sanad, M.F., Shalan, A.E., Bazid, S.M., et al, 2019. A graphene gold nanocomposite-based 5-FU drug and the enhancement of the MCF-7 cell line treatment. *RSC Adv.* 9, 31021–31029.
- Sathiyaseelan, A., Saravanakumar, K., Mariadoss, A.V.A., et al, 2021. pH-controlled nucleolin targeted release of dual drug from chitosan-gold based aptamer functionalized nano drug delivery system for improved glioblastoma treatment. *Carbohydr. Polym.* 262, 117907.
- Shi, Y., Goodisman, J., Dabrowiak, J.C., 2013. Cyclodextrin capped gold nanoparticles as a delivery vehicle for a prodrug of cisplatin. *Inorg. Chem.* 52, 9418–9426.
- Shinde, V.V., Jeong, D., Joo, S.W., et al, 2018. Mono-6-deoxy-6-aminopropylamino- β -cyclodextrin as a supramolecular catalyst for the synthesis of indolyl 1H-pyrrole via one-pot four component reaction in water. *Catal. Commun.* 103, 83–87.
- Siepmann, J., Siepmann, F., 2008. Mathematical modeling of drug delivery. *Int. J. Pharm.* 364, 328–343.
- Tarannum, N., Kumar, D., 2020. Synthesis, characterization and applications of copolymer of β -cyclodextrin: A review. *J. Polym. Res.* 27, 1–30.
- Vega, E., Egea, M.A., Calpena, A.C., et al, 2012. Role of hydroxypropyl- β -cyclodextrin on freeze-dried and gamma-irradiated PLGA and PLGA-PEG diblock copolymer nanospheres for ophthalmic flurbiprofen delivery. *Int. J. Nanomed.* 7, 1357.
- Yang, Q., Miyagawa, M., Liu, X., et al, 2018. Methyl- β -cyclodextrin potentiates the BITC-induced anti-cancer effect through modulation of the Akt phosphorylation in human colorectal cancer cells. *Biosci. Biotech. Bioch.* 82, 2158–2167.
- Zaghloul, N., El HOFFY, N.M., Mahmoud, A.A., et al, 2022. Cyclodextrin stabilized freeze-dried silica/chitosan nanoparticles for improved terconazole ocular bioavailability. *Pharmaceutics* 14, 470.